Structural adaptation of oxygen tolerance in 4-hydroxybutyrl-CoA dehydratase, a key enzyme of archaeal carbon fixation

Hasan DeMirci[1,2,3], **Bradley B. Tolar**[4], **Tzanko Doukov**[5], **Aldis Petriceks**[1], **Akshaye Pal**[1], **Yasuo Yoshikuni**[6], **David A. Saez**[7], **Juliana A. Murillo-López**[7], **Walter A. Rabanal-León**[8], **Esteban Vöhringer-Martinez**[7], **Thomas Schwander**[9], **Tobias J. Erb**[9], **Christopher A. Francis**[4], **Soichi Wakatsuki**[1,10]

1	Biosciences Division, SLAC National Accelerator Laboratory, Menlo Park, California, USA
2	Department of Molecular Biology and Genetics, Koc University, Sariyer, Istanbul, Turkey
3	Stanford PULSE Institute, SLAC National Accelerator Laboratory, Menlo Park, California, USA
4	Department of Earth System Science, Stanford University, Stanford, California, USA
5	Structural Molecular Biology, Stanford Synchrotron Radiation Lightsource, SLAC, Menlo Park, California, USA
6	DOE Joint Genome Institute, Lawrence Berkeley National Laboratory, Berkeley, California, USA
7	Departamento de Físico-Química, Facultad de Ciencias Químicas, Universidad de Concepción, Concepción, Chile
8	Departamento de Química Analítica e Inorgánica, Facultad de Ciencias Químicas, Universidad de Concepción, Concepción, Chile.
9	Max Planck Institute for Terrestrial Microbiology, Marburg, Germany
10	Department of Structural Biology, School of Medicine, Stanford University, Stanford, California, USA

Abstract

Autotrophic microorganisms that convert inorganic carbon into organic matter were key players in the evolution of life on early Earth. As the early atmosphere became oxygenated, these microorganisms needed protection from oxygen, which was especially important for those organisms that relied on enzymes with oxygen-sensitive metal clusters (e.g., Fe-S). Here we investigated how the key enzyme of the 3-hydroxypropionate/4-hydroxybutyrate (HP/HB) cycle for CO_2-fixation, 4-hydroxybutyryl-CoA dehydratase (4HBD), adapted from anoxic to oxic conditions. 4HBD is found in both anaerobic bacteria and aerobic ammonia-oxidizing archaea (AOA). The oxygen-sensitive bacterial 4HBD and oxygen-tolerant archaeal 4HBD share 59 % amino acid identity. To examine the structural basis of oxygen tolerance in archaeal 4HBD, we determined the atomic resolution structure of the enzyme. Two tunnels providing access to the canonical 4Fe-4S cluster in oxygen-sensitive bacterial 4HBD were closed with four conserved mutations found in all aerobic AOA and other archaea. Further biochemical experiments support our findings that restricting access to the active site is key to oxygen tolerance, explaining how active site evolution drove a major evolutionary transition.

Introduction

The global carbon cycle and its biological influences have been deeply scrutinized as climate change intensifies [1]. This cycle – perturbed by excessive anthropogenic carbon emissions – affects biomass in ecosystems, ocean acidity, global temperatures, and numerous other global factors [1,2]. Therefore, understanding how nature both releases and sequesters carbon is key to addressing excess atmospheric carbon dioxide. Quantitatively, the assimilation of CO_2 into organic materials (and biomass) is the most important biosynthetic process. To date, six major CO_2-fixation pathways have been characterized [3–5]. These autotrophic pathways have similarities, but vary in kinetics, thermodynamics, enzymology, and oxygen tolerance, indicating adaptations to various environments or niches. Such adaptations in CO_2 fixation pathways impact fitness of autotrophic organisms, and therefore likely influenced the evolutionary divergence of early life [6,7]. Chemolithoautotrophic ammonia-oxidizing archaea (AOA) from the phylum *Thaumarchaeota* fix CO_2 using energy derived from the oxidation of ammonia - the first step in nitrification [8]. AOA flourish in the nutrient-poor open ocean, increasing in abundance with depth particularly below the photic zone [9], where they play a significant role in CO_2-fixation in the largest biome on Earth [10,11].

In order to thrive in oligotrophic environments, AOA require highly-efficient pathways especially those that initially convert inorganic carbon into biomass [12]. Appropriately, it was found that the first cultured representative of *Thaumarchaeota* - *Nitrosopumilus maritimus* - fixes CO_2 using a modified version of the 3-hydroxypropionate/4-hydroxybutyrate (HP/HB) cycle that was initially described in *Crenarcheaota* [13]. This thaumarchaeal HP/HB cycle variant is the most energy-efficient aerobic CO_2-fixation pathway presently known [3,13].

Though the benefits of a highly energy-efficient HP/HB cycle are clear, how this pathway and constituent enzymes evolved to adapt to dramatic changes in environmental conditions is much less understood. For example, one essential question is how *N. maritimus* was able to maintain such an efficient CO_2-fixation pathway as atmospheric oxygen concentrations increased to 20%. The answer may be found by investigating individual enzymes of the HP/HB cycle. In particular, 4-hydroxy-butyryl-CoA dehydratase (4HBD), as it is a key enzyme in both aerobic thaumarchaeal and crenarchaeal HP/HB cycles, and is also found in anaerobic bacteria. In the anaerobic bacterium *Clostridium aminobutyricum*, 4HBD catalyzes a key step in 4-aminobutyrate fermentation - the non-redox dehydration of a 4-hydroxybutyryl-CoA thioester to crotonyl-CoA [14] In Archaea, this reaction functions canonically in the second half of the HP/HB cycle, where succinyl-CoA is processed into two acetyl-CoA molecules. The enzyme requires FAD as a cofactor as well as a [4Fe-4S] cluster in the active site [15]. To date, structural and biochemical characterization of 4HBD has primarily focused on previously-known anaerobic versions, specifically in *C. aminobutyricum* [14–17]. More recently, a comparative functional characterization of 4HBD from anaerobic *C. aminobutyricum* and aerobic *N. maritimus* confirmed the stark difference in their oxygen sensitivity, ascribing it to a key evolutionary adaptation of AOA to an oxic environment [13]. However, since no high-resolution structure exists for the 4HBD from aerobic *Thaumarchaeota*, the mechanistic underpinnings behind

2

such adaptations remain unknown. In this study, we present the first high-resolution crystal structure of 4HBD from *N. maritimus*. This 4HBD structure shows for the first time, a substrate analogue bound at the active site, as well as one additional Fe atom between the [4Fe-4S] cluster and the substrate. Structural comparison with that of substrate-free *C. aminobutyricum* 4HBD as well as enzyme kinetics assays shed light on the co-evolution of 4HBD during the transition from the anoxic habitats of anaerobic bacteria to oxygenated environments inhabited by aerobic *Thaumarchaeota*.

Results

Unusual oxygen tolerance of purified *N. maritimus* 4HBD

It is well known that [4Fe-4S] cluster-containing proteins are very sensitive to the presence of oxygen, which typically necessitates the anaerobic production, purification, and characterization of these proteins. It was predicted and demonstrated *in vitro* that *N. maritimus* 4HBD has an unusually high oxygen tolerance with a half-life of more than 10 hours [13]. In our hands, purified 4HBD retained ~25% activity after prolonged incubation for several days under aerobic conditions, which made it possible to perform all purification steps of crystallization samples in the presence of oxygen. From purification to obtaining crystals typically takes 3-4 days. Crystals retained their dark brown color for a few weeks, suggesting that [4Fe-4S] cluster of 4HBD has unusual stability under ambient atmospheric conditions.

Overall Structure of *N. maritimus* 4HBD

In order to understand the molecular underpinnings of the catalytic mechanism of aerobic 4-Hydroxybutyryl-CoA dehydration, we determined the high-resolution *N. maritimus* 4HBD structure (encoded by Nmar_207) at 1.55 Å resolution. This structure shows an overall homotetrameric arrangement, which agrees with the previously reported structure of the oxygen-sensitive homolog from *C. aminobutyricum* (PDB ID 1U8V) (Figure 1). Each of the four monomers, referred to as A to D hereafter, contained an active site with one [4Fe-4S] cluster, an additional active site catalytic Fe atom, designated Fe-X (which has never before been structurally observed), and one FAD coenzyme molecule. The space group was $P12_11$. Monomers ranged from 500-502 residues, with 456-459 of those residues facing the surface. Four large monomer-monomer interfaces were present in this structure (between monomers A-C, A-D, B-C, and B-D), ranging from 3104 to 3271 $Å^2$, significant compared to the average surface area of isolated monomers ranging from 21,499 to 21,834 $Å^2$. The C-B and D-A interfaces were near-identical to one another; as were the D-B and C-A interfaces. The former interfaces both contained 35 hydrogen bonds, and a similar number of salt bridges (16 in C-A, 18 in D-B). The latter contained 27 and 28 hydrogen bonds, respectively, and 24 and 25 salt bridges.

Within each monomer, the most prominent secondary structures are α-helices (n = 21), primarily interspersed with regions of random coil. There also existed a few regions of short β-strands, the longest of which was only 8 residues in length (Figure 2). This is similar to the *C. aminobutyricum* 4HBD structure, with the N- and C-terminal regions consisting primarily of α-helical secondary structures interspersed with random coils, and the central domain (D168-S297) containing all of the protein's short β-strands (Figure 2).

The larger interfaces come together by flipping one of the two monomers from the symmetry axis by 180 degrees. In this conformation, the monomer-monomer interface is composed mainly of interactions between corresponding regions of α-helices and β-sheets.

Constriction of the tunnels behind the Fe-[4Fe-4S] cluster protecting oxygen attack

Further inspection of the structure of the oxygen tolerant *N. maritimus* 4HBD in comparison with that of the oxygen-sensitive 4HBD from *C. aminobutyricum* revealed that both enzymes feature two tunnels that expand from the active site to the back of the protein, but also showed striking differences (Figure 3A and B). The binding pocket for the Fe-[4Fe-4S] cluster is actually part of a 45 Å long tunnel ('tunnel 1'), which extends throughout the 4HBD monomer exiting at the other end of the protein (Figure 3B and D). Surprisingly, this tunnel is constricted severely halfway between the Fe-[4Fe-4S] and the other exit by a constellation of 6 residues, T102, Q237, G257, G258, R441, and N442 (Figure 3F). This constriction is as narrow as 2.7 Å in diameter, too small for oxygen molecules to pass. In addition to that, we observed that one water molecule at one side of the constriction makes hydrogen bonds to the carbonyl oxygen of R441, main chain nitrogen of G258, delta oxygen of N442, and epsilon oxygen of Q237. This water molecule apparently plugs the constriction site and serves as a barrier for molecular oxygen intrusion beyond this point, presumably preventing oxygen molecules from reaching the [4Fe-4S] cluster at the active site.

In contrast, the same tunnel in the oxygen-sensitive 4HBD from *C. aminobutyricum* is accessible all the way from the [4Fe-4S] cluster to the other end of the protein (Figure 3C), which is about 12 Å long and 4 to 5 Å wide. The tunnel is wide open at the position corresponding to the constriction of *N. maritimus* 4HBD. In *C. aminobutyricum* 4HBD, the cross section of the tunnel at this position is approximately 4 Å x 7 Å, surrounded by S98, Q233, G254, G255, A447, and S448. The striking differences are three residues, S98, A447 and S448 that are replaced by bulkier T102, R441 and N442, respectively, which constrict tunnel 1 in *N. maritimus* 4HBD (Figure 3E and 3F). These three residues are fully conserved in thaumarchaeal and crenarchaeal AOA (Figure 2 and Figure 4B) as well as *Plesiocystis pacifica*, which are all obligate (micro)aerobic microorganisms (Figure S4 of Berg et al. 2007)[18]. Other 4HBD sequences of anaerobic bacteria do not show strict conservation of these residues either, suggesting that 4HBD acquired oxygen tolerance by evolution of three residues to close the back entry of tunnel 1 to the active site. Mutation of the N442 to the corresponding serine of the anaerobic 4HBD, or an alanine, reduced the dehydration activity below 5% of the wild type. This loss of activity was observed under anaerobic conditions and did not

increase after exposure to air. Therefore, these mutations do not directly influence the oxygen-dependent inactivation, but might have a secondary effect on the active site.

In *C. aminobutyricum* 4HBD, the second tunnel ('tunnel 2') runs perpendicular to the first, immediately behind the [4Fe-4S] cluster (Figure 3A). The corresponding tunnel of *N. maritimus* 4HBD is interrupted in two places (Figure 3B). The one interruption closer to the back exit is closed completely by the side chain of L77, which corresponds to A73 in *C. aminobutyricum* 4HBD, while the other constriction closer to the [4Fe-4S] cluster is interrupted by overall structural changes near the constriction, not by specific mutations. The branched hydrophobic side chain of L77 sticks across back tunnel 2, and is conserved throughout aerobic AOA (Figure 2 and Figure 4B).

Active Site Architecture

The crystal structure of 4HBD reveals the first structure of an oxygen-sensitive archaeal dehydratase complex, to the best of our knowledge. The active site configuration is similar to that of *C. aminobutyricum*, with notable exception of the additional Fe-X that is only present in the *N. maritimus* structure. In both enzymes, the active site is accessed through a narrow binding channel near the surface of a monomer-monomer interface. The walls of this channel are formed by two interacting monomers. FAD rests in this channel, with its adenine ring proximal to the channel's entry while the isoalloxazine ring is facing the [4Fe-4S] cluster. (Figure 3A, 3B; Figure5A). The flavin moiety is tightly constrained in the active site. For example, in one A-C active site, FAD binds to monomer A at an interface of 512 Å^2, and monomer C at an interface of 525 Å^2.

An intriguing feature of the *N. maritimus* 4HBD structure is a substantial electron density near the Fe-X, its coordinating ligand residues (H295, Y299 and E449), and FAD. We hypothesize that this electron density corresponds to a substrate or product analogue. The substrate in this key dehydration reaction, 4-hydroxybutyryl-CoA, was also captured in our crystallized active site. This molecule was located near the isoalloxazine ring of FAD, and was stabilized by three hydrogen bonds at its 4' hydroxy position (H295, Y299, and E449, Figures 5C,D). In this position, the substrate has its CoA-thioester pointing toward the flavin moiety, leaving the 2' and 3' carbon positions directly above FAD. These results largely confirm prior characterizations of the *C. aminobutyricum* active site, which featured these three residues interacting with the substrate.

Interestingly, this FAD was not captured in a planar geometry. Instead, we observed a bending of the isoalloxazine ring of FAD at the nitrogen N5 position, similar to the butterfly shape observed in acyl-CoA dehydrogenases suggesting a shift in the electron potential of the cofactor [19].

Table 1. Distances between Fe-X and its ligands

Fe-X	Fe (cluster atom)	Glu449	His 295	Tyr299
Chain A	2.43	2.06	2.30	2.11
Chain B	2.61	2.08	2.30	2.13
Chain C	2.74	2.14	2.27	2.11
Chain D	2.26	2.09	2.38	2.09
QM-geometry	2.73	1.99	2.11	2.00

Measured distances in Å between catalytic Fe with Fe1 of the [4Fe-4S] cluster and H295-Y299-E449 triad (sidechain nitrogen of H295, hydroxyl oxygen of Y299, and carboxyl oxygen of E449). In the last row the distances from the QM/MM optimized geometry are shown.

Kinetics of active site variants

For the homologous anaerobic 4HBD from *C. aminobutyricum* it is reported that apart from the residues coordinating the [4Fe-4S] cluster (C99, C103, C299 and H292), four additional residues (T190, E257, Y296, and E455) are important for dehydratase activity [17]. Therefore, we introduced mutations in the corresponding residues of the *N. maritimus* 4HBD (T194, E260, Y299 and E449) and tested their kinetics. The high-resolution structure shows that E449 and Y299 interact with the Fe-X. The mutation of these residues to glutamine (E449Q) or phenylalanine (Y299F) respectively, drastically reduced the dehydration activity over 99% and the isomerization capability was also impaired.

Furthermore, E260 and T194 are proposed to form a diad involved in the protonation of the FAD semiquinone. Mutation of these residues to a glutamine (E260Q) or valine (T194V), respectively, significantly reduced the dehydration activity. The T194V variant was especially affected, since T194 is able to form a hydrogen bond with the N5 of the isoalloxazine ring.

We quantified the iron content of 4HBD. The results for the wild-type support the presence of an additional Fe atom as suggested from the high-resolution structure. Interestingly, the mutations in the Fe-X coordinating residues (Y299F and E449Q) reduced the iron content or overall protein stability. The mutations in the FAD interacting diad either had little influence on the iron content (E260Q) or impaired the oligomeric state of the enzyme (T194V), which resulted in a loss of iron.

Table 2. Characterization of wild-type and variants of 4HBD

4HBD	Dehydratation (4-hydroxybutyryl-CoA)			Isomerization (vinylacetyl-CoA)			Oligomeric state	Iron content per monomer
	Vmax (U/mg)	KM (µM)	Relative activity after 24h air (%)	Vmax (U/mg)	KM (µM)	Relative activity after 24h air (%)		
wt	20.4 ± 0.5	6.4 ± 0.8	91 ± 9	108 ± 2	318 ± 17	94 ± 4	tetrameric	4.4 ± 0.5***
E449Q	not detected	n.d.	n.d.	3.2 ± 0.3	1350 ± 230	109 ± 8	n.d.	n.d.
Y299F	0.10 ± 0.01	2.0 ± 0.2	4 ± 1 *	4.8 ± 0.2 **	141 ± 16	146 ± 6	tetrameric	3.9 ± 0.4
E260Q	0.85 ± 0.03	14.7 ± 1.8	92 ± 6	25 ± 3	318 ± 83	78 ± 6	tetrameric	4.2 ± 0.5
T194V	not detected	n.d.	n.d.	10 ± 1	284 ± 26	116 ± 8	tetrameric /dimeric	3.1 ± 0.4

n.d. = not determined. * 89 ± 3 % activity retention under anaerobic conditions. ** Substrate inhibition with a Ki of 1700 ± 500 µM. *** results the WT were obtained from three individual enzyme preparations while those of the mutants were obtained from three measurements on single preparations.

Discussion

Comparison of the substrate binding pockets with the bacterial counterpart

The overall structures of (aerobic) archaeal 4HBD from *N. maritimus* and the (anaerobic) bacterial homolog from *C. aminobutyricum* show a very similar architecture with RMSD of 0.54 Å between 14,738 atoms with minor differences (Supplementary Figure S1A). The *N. maritimus* 4HBD sequence has an additional 6 N-terminal residues and 24 additional C-terminal residues, while *C. aminobutyricum* 4HBD has 8 residues inserted between helices α11 and α12. These N- and C-terminal extensions of the *N. maritimus* enzyme neither affect the oligomeric state nor the overall conformational state of the 4HBD. The active sites of the two homologous enzymes, despite their differences for oxygen tolerance, display a striking similarity. Position of the critical catalytic residues E449, Y299, H295, FAD and the [4Fe-4S] cluster are highly conserved (Figure 2). The only major difference is the existence and coordination of an active site Fe atom in *N. maritimus* 4HBD which may protect the [4Fe-4S] cluster in the presence of oxygen. In addition to the ~58% sequence identity, the two 4HBD enzymes also share a remarkably similar surface charge distribution (Supplementary Figure S1 C,D).

Oxygen tolerance acquired by blocking tunnels in proteins

It has been reported that blocking a protein tunnel is essential for protection in a pair of oxygen-tolerant and -sensitive [NiFe]-hydrogenases [20–22]. The oxygen-tolerant enzyme features a

tunnel that is blocked by a tryptophan at the position of the medial 3Fe-4S cluster tunnel, while the oxygen-sensitive hydrogenase has a smaller residue, phenylalanine, which does not fully close the tunnel. This situation resembles somewhat the case of the alanine to leucine mutation of tunnel 2 in 4HBD (Figure 3 A,B). In contrast, the constriction of tunnel 1 requires three mutations, S98 to T102, A447 to R441, and S442 to N442. To analyze the rigidity in the constriction of tunnel 1, we calculated the mechanical strength of the residues using the program ProPHet [23–25] (http://bioserv.rpbs.univ-paris-diderot.fr/services/ProPHet/). Overall, this analysis suggests that the three residues constricting tunnel 1 show above-threshold mechanical strength (Supplementary Figure S2) indicating that the constriction is rather sturdy.

It is not clear why 4HBDs feature such extensive tunnels at the back of their active sites containing the [4Fe-4S] clusters. Martins et al. (2004) [15] and Zhang et al (2015) [17] alluded to one of the back tunnels (tunnel 1) of *C. aminobutyricum* 4HBD as a possible escape route for the product water, but did not discuss the possible diffusion of oxygen through the two tunnels. Our structural and phylogenetic analyses of *N. maritimus* 4HBD in comparison with its oxygen-sensitive counterpart, *C. aminobutyricum* 4HBD, suggest that the 4 residues co-evolved together to close the two tunnels, probably protecting the active site of *N. maritimus* 4HBD (and other oxygen-tolerant enzymes) from an attack by oxygen. However, another possible route for oxygen to reach the active site is through the front tunnel, which is open when no substrate or product is bound. The role of the additional Fe atom, Fe-X in front of the [4Fe-4S] cluster remains unclear at this stage but it is tempting to speculate that the Fe-X could play a role of a gatekeeper against oxygen attack through the front tunnel.

Confirmation of Fe-X stability by quantum chemical energy calculations

The anomalous difference map from the diffraction data collected at the Fe K-edge clearly shows a very strong (above 5 σ) Fe peak. The anomalous difference map also shows the Fe atoms of the [4Fe-4S] cluster at a much lower σ level (data not shown). The fifth is tightly coordinated by Fe1 of the [4Fe-4S] cluster and the conserved triad H295-Y299-E449 (Table 1), and leaves very little space for oxygen molecules to pass by to reach the [4Fe-4S] cluster (Figure 3D), thus potentially protecting the cluster from oxygen attack, even when no substrate is bound in the active site. Another role of the Fe-X could be a novel Fe-S cluster, Fe-[4Fe-4S]. There are examples of other similar exotic Fe-S clusters, such as the C cluster [Ni-4Fe-4S] of carbon monoxide dehydrogenase [26,27]. In the case of *N. maritimus* 4HBD, however, the x-ray fluorescence spectroscopy of the crystals and anomalous map analysis showed no Ni signals, excluding the possibility of a [Ni-4Fe-4S] cluster. The kinetics experiments of the Fe-X liganding residues showed clearly the significant inactivation by oxygen of the enzyme upon mutations of these residues (Table 2), corroborating the potential importance of the Fe-X atom at that position and its potential role as protector of the [4Fe-4S] cluster against oxygen. Is there a possibility that this Fe-X could be one of the Fe atoms of the [4Fe-4S] cluster displaced when the cluster is partially oxidized? For example, a 1.8 Å shift of Fe atom

was observed in the proximal [4Fe-4S] cluster in [NiFe]-hydrogenase of Group 1c (Hyb-type) from *Citrobacter* sp. S-77 by Higuch *et al.* who showed that the [4Fe-4s] cluster is distorted in the oxidized form and the Fe4 atom is shifted by 1.8 Å towards its ligand, an aspartate sidechain oxygen, concomitant with a displacement of S1 sulfur (Figure 2B and Figure S2F of Noor (2018) [28]). They have proposed that the displaced Fe4 serves to protect the active site from O_2.

To investigate if the Fe-X is stable at that observed position in front of the [4Fe-4S] cluster, we pursued quantum chemical energy calculations starting with the high-resolution structure of the *N. maritimus* 4HBD. We equilibrated the tetramer in aqueous solution at 298K and 1 bar using all-atom molecular dynamics simulations applying restraints on the active site atoms. The last structure of the trajectory was then used to optimize the geometry of the active site in chain D of the tetramer quantum mechanically (BP86/def2-svp level of theory) applying the electrostatic embedding and the link atom method, which accounts for the electrostatic effect of the surrounding protein. We obtained a minimum on the potential energy surface, in which Fe-X coordinates to the conserved residue triad (H295-Y299-E449) and the nearest Fe atom of [4Fe-4S] cluster (Figure 5E). In the energy minimized 4HBD structure, the [4Fe-4S] cluster has an almost symmetric geometry. The Fe-X atom has a distance of 2.7 Å to the iron atom Fe1 of the [4Fe-4S] cluster (Table 1 last row), similar to the observed distances in the crystal structure, 2.4 to 2.7 Å. The distance of 2.7 Å is substantially longer than the 1.8 Å shift of Fe4 between the oxidized and reduced forms of the hydrogenase of Group 1c (Hyb-type) from *Citrobacter* sp. S-77 mentioned above [28]. The position of FAD in the active site favors a possible transfer of electrons or protons to a putative substrate or the [4Fe-4S] cluster associated with the reaction. Further elucidation of the role of the Fe-X in relation to the [4Fe-4S] cluster would require much more sophisticated analysis, such as in-crystal electron paramagnetic resonance and extended x-ray absorption fine structure analysis of crystalline enzymes.

Concluding remarks

Although initially described in obligately anaerobic bacteria, 4HBD has been found in many aerobic Archaea [3,13]. Though the phylogeny of crenarchaeal 4HBD used in the HP/HB cycle forms two distinct groups, all thaumarchaeal 4HBD protein sequences cluster together in a separate clade. This clade is most closely related to 4HBD from anaerobic bacteria (including *C. aminobutyricum*), indicating that evolution of the HP/HB cycle likely occurred twice in the Archaea [13]. In contrast to anaerobic 4HBD, oxygen tolerance has been observed both with *N. maritimus* 4HBD and *Metallosphaera sedula* - a member of the Crenarchaeota [13,29]. If 4HBD originated in anaerobic bacteria, then it appears that Archaea not only acquired the enzyme on two separate occasions, but also managed to convert the enzyme to a more oxygen-tolerant form twice. A structural comparison of 4HBD from *M. sedula* would allow identification of such modifications and potentially give insight for future bioengineering efforts. For now, we can observe that the kinetics of 4HBD enzyme activity (K_m, V_{max}) are nearly identical in *C. aminobutyricum* and *N. maritimus* [13], whereas the K_m of *M. sedula* 4HBD is 2-3 times higher and its V_{max} is lower by a factor of 10 [29].

The apparent impact of oxygen on the evolution of the HP/HB cycle is further supported by the notion that evolution of Thaumarchaeota coincided with the introduction of oxygen into the atmosphere and ocean in Earth's past [30]. Through lateral gene transfer, bacteria contributed key genes including 4HBD to the Thaumarchaeota. Even more interestingly, the gain of HP/HB cycle genes among AOA is distinct from non-AOA Thaumarchaeota and this divergence also included the gain of ammonia oxidation and cobalamin (vitamin B_{12}) biosynthesis genes - hallmarks of AOA metabolism [30].

Within the AOA, distinct phylogenetic groupings that match environmental habitat have been described, referred to as ecotypes, for terrestrial, freshwater, and shallow and deep marine Thaumarchaeota [31]. These groups are thought to have diverged from one another through a series of adaptations to their environment, although specific markers have not been identified. Some interesting insights include the gain of potassium transport for marine clades, whereas terrestrial AOA gained oxidative stress response genes [30]. Through this diversification, key metabolic genes would also have changed, which is reflected in the enzyme kinetic differences observed between the marine (*N. maritimus*) and terrestrial ammonia monooxygenases [12,32]. Similar changes are likely in HP/HB cycle enzymes. Therefore, by taking a structural biology approach [33] to investigating enzymes like 4HBD in ecologically-relevant organisms (including the five AOA ecotypes highlighted in Figure 2), we can gain a better understanding of evolution and adaptation of key enzymes in the global carbon cycle to changing environments as will be experienced with climate change.

Considering the impact of rising atmospheric CO_2 on global climate, structural knowledge of this enzyme may prove valuable for future endeavors to address climate change by engineering natural or synthetic enzymes and pathways for the capture and conversion of CO_2 that are more efficient than natural evolved ones [34]. Understanding the molecular basis of oxygen tolerance in one of the key enzymes of the HP/HB cycle for CO2-fixation will be useful for any future engineering efforts that may form the basis for development of effective bio-based carbon sequestration technologies.

Experimental procedures

Cloning

The gene encoding 4-hydroxybutyryl-CoA dehydratase (4HBD; Nmar_207) was purchased from Genscript Biotech (codon-optimized with cleavable N-terminal hexa-Histidine tag). Within the gene, *Nde*I and *BamH*I endonuclease restriction sites were used to insert Nmar_207 into the pET28a vector plasmid. The plasmid was transformed into E. *coli* strain BL21 (Rosetta-2), from EMD Millipore. Transformed *E. coli* were then grown overnight on agar plates (50 µg/ml kanamycin, 30 µg/ml chloramphenicol) at 37 °C.

10

Protein Expression and Purification

Overnight cultures started with single colonies from agar plates in LB media supplemented with 50 µg/ml kanamycin, 30 µg/ml chloramphenicol. They were diluted 1:100 into 12 x 2 L (total 24 L) cultures for large-scale protein expression and purification. After cultures reached an optical density of 0.8 at 600 nm, IPTG (final concentration 0.7 µM) was added to induce protein expression. Cultures were incubated overnight at 16 °C, and cell pastes were collected via centrifugation 30 mins at 4000g. The cells were resuspended in lysis buffer containing (50 mM TRIS HCl pH 7.0, 1 M KCl, 5 % v/v glycerol and 0.01 % triton X100) and sonicated by Branson Sonifier at 60% about 20 seconds three times (Branson Ultrasonics, Danbury, CT). Following the sonication, a second centrifugation was performed by using Beckman L8M ultracentrifuge equipped with Ti45 rotor (Beckman Coulter, Palo Alto, CA) at 4 °C and 40,000 g for 30 mins, soluble protein solution was acquired and kept at 4 °C for the rest of the purification. Protein purity and amount was estimated through SDS-PAGE.

Protein was further purified using FPLC; Ni-NTA column packed with 20 ml of Ni-NTA resin (Qiagen). The Ni-NTA column was first washed with loading buffer A (20 mM TRIS-HCl pH 7.0, 300 mM NaCl), and the bound protein was eluted in elution buffer B (500 mM imidazole, 300 mM NaCl, 50 mM TRIS, pH 7.0). Thrombin was then added to remove N-terminal cleavable hexa-histidine tag. The cleaved protein was then concentrated to 2.0 ml final concentration and loaded on the S200 column (GE healthcare). S200 size exclusion chromatography has yielded a single peak around 230 KDa, eluting at the tetrameric size 4HBD. Fractions collected, pooled and concentrated by ultrafiltration using Amicon 30 KDa size filters and quantity was measured using UV-Vis absorption spectroscopy at 280 nm. The final concentration of the protein solution was 10 mg/ml – confirmed by Nanodrop UV spectra (280 nm).

Crystallization

For initial crystallization screens 1 µl protein solution was added to crystal screen conditions in Terasaki plates (BioExpress), in 1:1 (v/v) ratio and sitting drop geometry. The sitting drop was then covered with 20 µl of parafin oil. Initial microcrystals were obtained by extensive pre-screening with all commercially available crystallization screens at ambient temperature. Best crystals exclusively obtained by using Molecular Dimensions' Midas screen from conditions containing 0.1 M Li_2SO_4, 0.1 M Tris, pH 8 with 25 % v/v Jeffamine ED-2003.

To prepare for diffraction experiments, crystals were soaked overnight in 2.5 µl of 33 % MPD as cryoprotectant (v/v) and 77 % (v/v) mother liquor. Following cryoprotection, crystals were flash-frozen quickly plunging them in liquid nitrogen.

X-ray Diffraction Data Collection

X-ray diffraction data for 4HBD crystals were collected on a Pilatus 6M detector at the BL12-2 beamline of the Stanford Synchrotron Radiation Light Source in Menlo Park, CA at a wavelength

of 0.979 Å and -180 °C. Diffraction data for 4HBD in space group P2$_1$ were collected to 1.55 Å resolution with cell dimensions a=87.530 Å b= 72.954 Å c=180.517 Å α=90.00 β=98.38 γ=90.00 . A single crystal was used for the 4HBD dataset. The diffraction images were processed and scaled using the *HKL2000* package [35]. The data processing statistics are summarized in Supplementary Table S1.

Structure Determination and Refinement

The RsmF structure was solved by molecular replacement with the program *PHASER* [36,37] from the *CCP4* program suite [38] in space group P2$_1$ to 1.55 Å resolution. The initial search model was built with the program *MODELLER* [39] from one of the four subunits of anaerobic *C. aminobutyricum* 4HBD (PDB ID 1u8v). After the placement of 4 of 4HBD subunits in the asymmetric unit and initial refinement with PHENIX [40], the model was further rebuilt with *ARP/wARP* [41]. The resulting model was 95% complete and manually checked and completed with Coot [42,43]. Final crystallographic refinement was performed with the program *PHENIX* [40]. The crystallographic R/ R$_{free}$ factors are 0.157/0.175 for the 4HBD dataset respectively. The stereochemical quality of the model was assessed with Procheck [44]. The Ramachandran statistics (most favored/ additionally allowed/ generously allowed/ disallowed) are 92.5/7.5/0.0/0.0 % . The refinement statistics are summarized in Supplementary Table S1. Figures were generated using *PyMOL* [45].

Enzyme activity assays

Dehydration activity was measured aerobically in 120 µl of 100 mM MOPS pH 7.5 buffer containing 0.2 mM NADPH, 1 µg enoyl-thioester reductase (Etr1p) and either 0.032 µg 4HBD, 15 µg E449Q, 16 µg Y299F, 3.5 µg E260Q or 15 µg T194V. The reaction was started with different concentrations of 4-hydroxybutyryl-CoA (synthesized according to the protocol by Könneke, M. *et al* [13]) and the consumption of NADPH was followed at 30 °C and 340 nm (Δε=6.22 mM-1 cm-1) with a Cary 60 UV-Vis spectrophotometer (Agilent Technologies, Germany).

Isomerization activity was measured aerobically in 120 µl of 100 mM MOPS pH 7.5 buffer containing 0.2 mM NADPH, 2 mM acetyl-CoA, 1 µg enoyl-thioester reductase (Etr1p), 7.6 µg 4-hydroxybutyrate CoA-transferase (AbfT) and either 0.032 µg 4HBD, 0.6 µg E449Q, 0.21 µg Y299F, 0.35 µg E260Q or 0.45 µg T194V. The reaction was started with different concentrations of 3-butenoic acid and the consumption of NADPH was followed at 30 °C and 340 nm (Δε=6.22mM-1cm-1) with a Cary 60 UV-Vis spectrophotometer (Agilent Technologies, Germany).

To test the activity after exposure to air, the enzyme was prepared under anaerobic conditions. The initial activity was measured with the assay described above, with the substrate concentration fixed to 160 µM 4-hydroxybutyryl-CoA or 1000 µM 3-butenoic acid respectively. The enzyme stocks were split, and kept at room temperature under anaerobic or aerobic conditions for 24 h. Afterwards, activity of the anaerobic and aerobic aliquot were re-measured.

Iron quantification

The iron content of 4HBD and variants was determined by applying a modified method W.W. Fish [46]. 100 μL protein solution was hydrolyzed at 65 °C with the addition of 50 μL solution A (0.6 N HCl and 2.25 % w/v $KMnO_4$), until the mixture turns transparent. Afterwards, 10 μL solution B (6.5 mM ferrozine, 13.1 mM neocuproine, 2 M ascorbic acid and 5 M ammonium acetate) was added and incubated for 20 min at room temperature. To obtain a standard curve, the same procedure was applied for samples containing a defined concentration of Iron(II) ethylenediammonium sulfate tetrahydrate. The iron concentration was obtained by measuring the absorbance at 562 nm in a 96-well plate reader (Tecan, Switzerland) and calculating the concentration from the standard curve.

Phylogenetic Analysis

We first performed a BLASTP analysis using the *N. maritimus* 4HBD as a query and retrieved all sequences. We then eliminated the sequences that have length shorter than 80% of *N. maritimus* 4HBD and over 90% identity to any other sequences in the list using CD-HIT (https://www.bioinformatics.org/cd-hit/)[47]. We finally performed multiple sequencing alignment and tree construction with MUSCLE and FastTree [48] using their default parameters. The proportions of the amino acids are plotted with R using ggseqlogo (https://omarwagih.github.io/ggseqlogo/).

Computational optimization of active site geometry

The tetrameric crystal structure coordinates were solvated in an electrically neutral octahedral box of TIP3P water, leaving 1 nm between the edge of box and the closest atom of the solute. The iron-sulfur cluster and its surrounding cysteines were modeled using the parameters provided by Blachly et *al.* [49]. The force field parameters to describe FAD were taken from the GAFF force field. The additional iron atom was modeled as a divalent cation. The solvated system was subject to energy minimization constraining the position of the cluster, the surrounding cysteines, FAD, Fe-X and its coordinating residues adding an aspartate residue coordinating to H295 and lysine residue to E449. Then, the system was gradually heated from an initial temperature of 100 K to 300 K, constraining all solute (protein+ligand) atoms and equilibrated during 1 ns under NPT conditions (1 bar and 300 K) using the MonteCarlo barostat. Finally, 1 ns of NVT dynamics was performed constraining the cluster and surrounding residues, but releasing the rest of the protein. All simulations were done with the AMBER16 package [50].

From the final equilibrated structure an active site model was created with all residues shown in Figgure 5e applying the link atom technique to saturate the valence and including the rest of the protein or solvent atoms in a 3 nm radius as point charges in the quantum chemical calculations with the ORCA 4.1 package [51]. During the optimization at the BP86/def2-svp level the FAD molecule and the protein residue were kept fixed whereas the Fe-X, the coordinating residues and the [4Fe-4S] cluster were free to move. The triplet state was the lowest energy state for the optimized geometry of the system consisting of more than 100 atoms compared to the singlet state

(BP86/def2-TZVP). The employed level of theory has been shown to be adequate to find minimum energy geometries of [4Fe-4S] system compared to other DFT methods [52].

Data Availability

Coordinates of the four 4HBD structure have been deposited in the Protein Data Bank under accession code 6VJR.

Acknowledgments

Conflict of interest

Authors declare that they have no conflicts of interest regarding the results described in the manuscript.

Author contributions

H.D., B.T., C.F., and S.W. designed and coordinated the project. H.D. prepared and characterized the samples. H.D., T.D. and S.W. analyzed data. T.S. performed kinetics experiments. H.D., T.D., A.P. helped with data collection. D.S performed the molecular dynamics simulations and J.M the QM simulations and analyzed the data, W.R. helped in setting up QM calculations, E.V-M. coordinated the calculations, analyzed the data. H.D., B.T., C.F., TJE, E.V-M, and S.W. wrote the manuscript with input from all of the authors.

References

1. Seinfeld, J. H. & Pandis, S. N. *ATMOSPHERIC CHEMISTRY AND PHYSICS From Air Pollution to Climate Change SECOND EDITION. 2nd edition. Wiley, Chichester.* (2006). doi:10.1016/0016-7037

2. Liu, S. *et al.* Response of soil carbon dioxide fluxes, soil organic carbon and microbial biomass carbon to biochar amendment: a meta-analysis. *GCB Bioenergy* **8**, 392–406 (2016).

3. Berg, I. A. Ecological Aspects of the Distribution of Different Autotrophic CO 2 Fixation Pathways. *Appl. Environ. Microbiol.* **77**, 1925–1936 (2011).

4. Erb, T. J. Carboxylases in natural and synthetic microbial pathways. *Applied and Environmental Microbiology* (2011). doi:10.1128/AEM.05702-11

5. Offre, P., Spang, A. & Schleper, C. Archaea in biogeochemical cycles. *Annu. Rev. Microbiol.* **67**, 437–57 (2013).

6. Braakman, R. & Smith, E. The emergence and early evolution of biological carbon-fixation. *PLoS Comput. Biol.* (2012). doi:10.1371/journal.pcbi.1002455

7. Fuchs, G. Alternative Pathways of Carbon Dioxide Fixation: Insights into the Early Evolution of Life? *Annu. Rev. Microbiol.* (2011). doi:10.1146/annurev-micro-090110-102801

8. Könneke, M. *et al.* Isolation of an autotrophic ammonia-oxidizing marine archaeon. *Nature* **437**, 543–546 (2005).

9. Karner, M. B., Delong, E. F. & Karl, D. M. Archaeal dominance in the mesopelagic zone of the Pacific Ocean. *Nature* (2001). doi:10.1038/35054051

10. Wuchter, C. *et al.* Archaeal nitrification in the ocean. *Proc. Natl. Acad. Sci. U. S. A.* (2006). doi:10.1073/pnas.0600756103

11. Ingalls, A. E. *et al.* Quantifying archaeal community autotrophy in the mesopelagic ocean usinq natural radiocarbon. *Proc. Natl. Acad. Sci. U. S. A.* (2006). doi:10.1073/pnas.0510157103

12. Martens-Habbena, W., Berube, P. M., Urakawa, H., De La Torre, J. R. & Stahl, D. A. Ammonia oxidation kinetics determine niche separation of nitrifying Archaea and Bacteria. *Nature* (2009). doi:10.1038/nature08465

13. Könneke, M. *et al.* Ammonia-oxidizing archaea use the most energy-efficient aerobic pathway for CO2 fixation. *Proc. Natl. Acad. Sci. U. S. A.* (2014). doi:10.1073/pnas.1402028111

14. SCHERF, U. & BUCKEL, W. Purification and properties of an iron-sulfur and FAD-containing 4-hydroxybutyryl-CoA dehydratase/vinylacetyl-CoA3-2-isomerase from Clostridium aminobutyricum. *Eur. J. Biochem.* **215**, 421–429 (1993).

15. Martins, B. M., Dobbek, H., Çinkaya, I., Buckel, W. & Messerschmidt, A. Crystal structure of 4-hydroxybutyryl-CoA dehydratase: Radical catalysis involving a [4Fe-4S] cluster and flavin. *Proc. Natl. Acad. Sci. U. S. A.* (2004). doi:10.1073/pnas.0403952101

16. Gerhardt, A., Çinkaya, I., Linder, D., Huisman, G. & Buckel, W. Fermentation of 4-aminobutyrate by Clostridium aminobutyricum : cloning of two genes involved in the formation and dehydration of 4-hydroxybutyryl-CoA. *Arch. Microbiol.* **174**, 189–199 (2000).

17. Zhang, J., Friedrich, P., Pierik, A. J., Martins, B. M. & Buckel, W. Substrate-induced radical formation in 4-hydroxybutyryl coenzyme a dehydratase from Clostridium aminobutyricum. *Appl. Environ. Microbiol.* (2015). doi:10.1128/AEM.03099-14

18. Berg, I. A., Kockelkorn, D., Buckel, W. & Fuchs, G. A 3-hydroxypropionate/4-hydroxybutyrate

autotrophic carbon dioxide assimilation pathway in archaea. *Science* **318**, 1782-1786 (2007). doi:10.1126/science.1149976

19. Schwander, T., McLean, R., Zarzycki, J. & Erb, T. J. Structural basis for substrate specificity of methylsuccinyl-CoA dehydrogenase, an unusual member of the acyl-CoA dehydrogenase family. *J. Biol. Chem.* **293**, 1702–1712 (2018).

20. Fritsch, J. *et al.* The crystal structure of an oxygen-tolerant hydrogenase uncovers a novel iron-sulphur centre. *Nature* **479**, 249–252 (2011).

21. Montet, Y. *et al.* Gas access to the active site of Ni-Fe hydrogenases probed by X-ray crystallography and molecular dynamics. *Nat. Struct. Biol.* (1997). doi:10.1038/nsb0797-523

22. Kalms, J. *et al.* Krypton Derivatization of an O2-Tolerant Membrane-Bound [NiFe] Hydrogenase Reveals a Hydrophobic Tunnel Network for Gas Transport. *Angew. Chemie - Int. Ed.* (2016). doi:10.1002/anie.201508976

23. Lavery, R. & Sacquin-Mora, S. Protein mechanics: A route from structure to function. in *Journal of Biosciences* (2007). doi:10.1007/s12038-007-0089-x

24. Sacquin-Mora, S., Laforet, É. & Lavery, R. Locating the active sites of enzymes using mechanical properties. *Proteins Struct. Funct. Bioinforma.* **67**, 350–359 (2007).

25. Bocahut, A., Bernad, S., Sebban, P. & Sacquin-Mora, S. Frontier Residues Lining Globin Internal Cavities Present Specific Mechanical Properties. *J. Am. Chem. Soc.* **133**, 8753–8761 (2011).

26. Darnault, C. *et al.* Ni-Zn-[Fe4-S4] and Ni-Ni-[Fe4-S4] clusters in closed and open α subunits of acetyl-CoA synthase/carbon monoxide dehydrogenase. *Nat. Struct. Mol. Biol.* **10**, 271–279 (2003).

27. Doukov, T. I., Blasiak, L. C., Seravalli, J., Ragsdale, S. W. & Drennan, C. L. Xenon in and at the end of the tunnel of bifunctional carbon monoxide dehydrogenase/acetyl-CoA synthase. *Biochemistry* (2008). doi:10.1021/bi702386t

28. Noor, N. D. M. *et al.* Redox-dependent conformational changes of a proximal [4Fe–4S] cluster in Hyb-type [NiFe]-hydrogenase to protect the active site from O 2. *Chem. Commun.* **54**, 12385–12388 (2018).

29. Hawkins, A. B., Adams, M. W. W. & Kelly, R. M. Conversion of 4-hydroxybutyrate to acetyl coenzyme A and its anapleurosis in the Metallosphaera sedula 3-hydroxypropionate/4-hydroxybutyrate carbon fixation pathway. *Appl. Environ. Microbiol.* (2014). doi:10.1128/AEM.04146-13

30. Ren, M. *et al.* Phylogenomics suggests oxygen availability as a driving force in Thaumarchaeota evolution. *ISME J.* (2019). doi:10.1038/s41396-019-0418-8

31. Biller, S. J., Mosier, A. C., Wells, G. F. & Francis, C. A. Global Biodiversity of Aquatic Ammonia-Oxidizing Archaea is Partitioned by Habitat. *Front. Microbiol.* **3**, (2012).

32. Dimitri Kits, K. *et al.* Kinetic analysis of a complete nitrifier reveals an oligotrophic lifestyle. *Nature* (2017). doi:10.1038/nature23679

33. Tolar, B. B. *et al.* Integrated structural biology and molecular ecology of N-cycling enzymes from ammonia-oxidizing archaea. *Environmental Microbiology Reports* (2017). doi:10.1111/1758-2229.12567

34. Schwander, T., Schada von Borzyskowski, L., Burgener, S., Cortina, N. S. & Erb, T. J. A synthetic pathway for the fixation of carbon dioxide in vitro. *Science* **354**, 900–904 (2016).

35. Minor, W., Cymborowski, M. & Otwinowski, Z. Automatic system for crystallographic data

collection and analysis. *Acta Phys. Pol. A* (2002). doi:10.12693/APhysPolA.101.613

36. McCoy, A. J. *et al.* Phaser crystallographic software. *J. Appl. Crystallogr.* (2007). doi:10.1107/S0021889807021206

37. McCoy, A. J. Acknowledging Errors: Advanced Molecular Replacement with Phaser. in *Methods in Molecular Biology* 421–453 (2017). doi:10.1007/978-1-4939-7000-1_18

38. Winn, M. D. *et al.* Overview of the CCP4 suite and current developments. *Acta Crystallographica Section D: Biological Crystallography* (2011). doi:10.1107/S0907444910045749

39. Webb, B. & Sali, A. Protein structure modeling with MODELLER. in *Methods in Molecular Biology* (2017). doi:10.1007/978-1-4939-7231-9_4

40. Adams, P. D. *et al.* PHENIX : a comprehensive Python-based system for macromolecular structure solution. *Acta Crystallogr. Sect. D Biol. Crystallogr.* **66**, 213–221 (2010).

41. Langer, G., Cohen, S. X., Lamzin, V. S. & Perrakis, A. Automated macromolecular model building for X-ray crystallography using ARP/wARP version 7. *Nat. Protoc.* (2008). doi:10.1038/nprot.2008.91

42. Emsley, P., Lohkamp, B., Scott, W. G. & Cowtan, K. Features and development of Coot . *Acta Crystallogr. Sect. D Biol. Crystallogr.* (2010). doi:10.1107/s0907444910007493

43. Emsley, P. & Cowtan, K. Coot: Model-building tools for molecular graphics. *Acta Crystallogr. Sect. D Biol. Crystallogr.* (2004). doi:10.1107/S0907444904019158

44. Laskowski, R. A., MacArthur, M. W., Moss, D. S. & Thornton, J. M. PROCHECK: a program to check the stereochemical quality of protein structures. *J. Appl. Crystallogr.* (1993). doi:10.1107/s0021889892009944

45. DeLano, W. L. References. *Hypertens. Res.* **37**, 362–387 (2014).

46. Fish, W. W. Rapid Colorimetric Micromethod for the Quantitation of Complexed Iron in Biological Samples. *Methods Enzymol.* (1988). doi:10.1016/0076-6879(88)58067-9

47. Li, W. & Godzik, A. Cd-hit: a fast program for clustering and comparing large sets of protein or nucleotide sequences. *Bioinformatics* **22**, 1658–1659 (2006).

48. Price, M. N., Dehal, P. S. & Arkin, A. P. FastTree 2 - Approximately maximum-likelihood trees for large alignments. *PLoS One* (2010). doi:10.1371/journal.pone.0009490

49. Blachly, P. G., de Oliveira, C. A. F., Williams, S. L. & McCammon, J. A. Utilizing a Dynamical Description of IspH to Aid in the Development of Novel Antimicrobial Drugs. *PLoS Comput. Biol.* (2013). doi:10.1371/journal.pcbi.1003395

50. Case, D. A. *et al.* Amber 2017. *Univ. California, San Fr.* (2017). doi:citeulike-article-id:2734527

51. Neese, F. The ORCA program system. *Wiley Interdiscip. Rev. Comput. Mol. Sci.* (2012). doi:10.1002/wcms.81

52. Harris, T. V. & Szilagyi, R. K. Iron–sulfur bond covalency from electronic structure calculations for classical iron–sulfur clusters. *J. Comput. Chem.* **35**, 540–552 (2014).
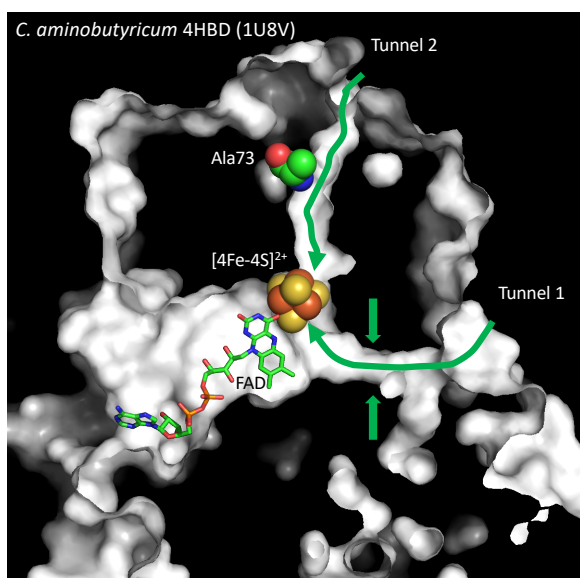
FIGURES:
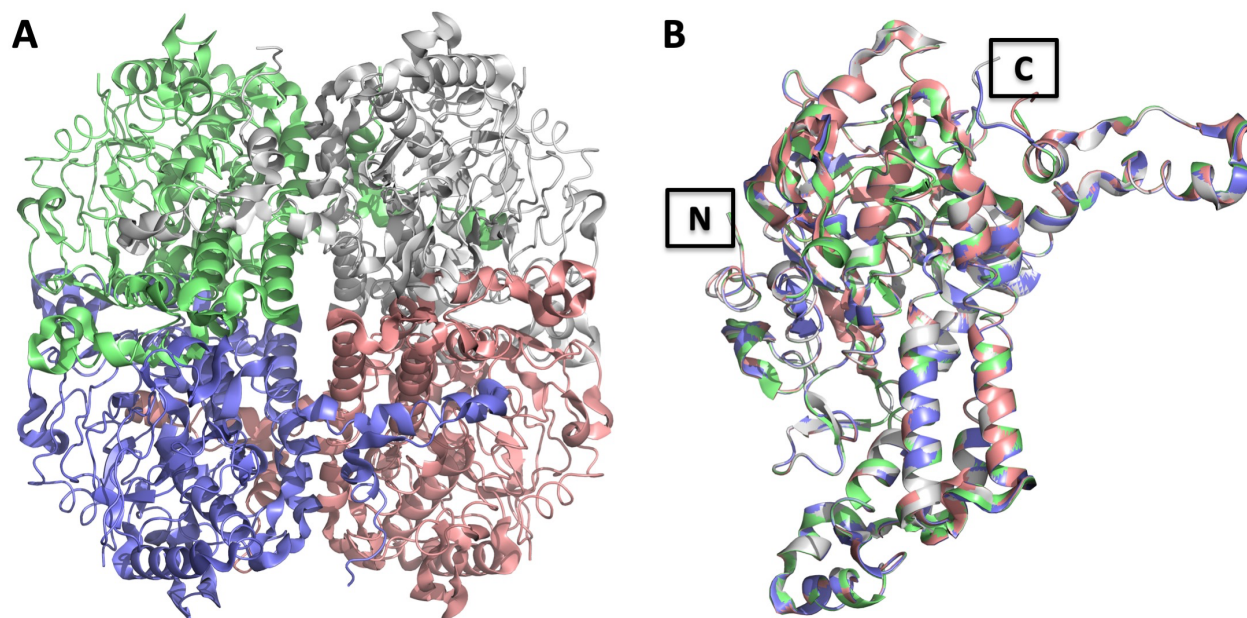
Figure 1. Overall structure of the *N. maritimus* 4-hydroxybutyryl-CoA dehydratase (4HBD). A) Cartoon representation of the 4HBD homotetramer. Each chain is shown in a different color. B) Superposition of all four monomers indicates the overall similarity and structural conformation of each with an overall root mean square deviation (RMSD) of 0.07-0.09 Å. The positions of the N- and C-termini of the subunits are indicated with black squares.
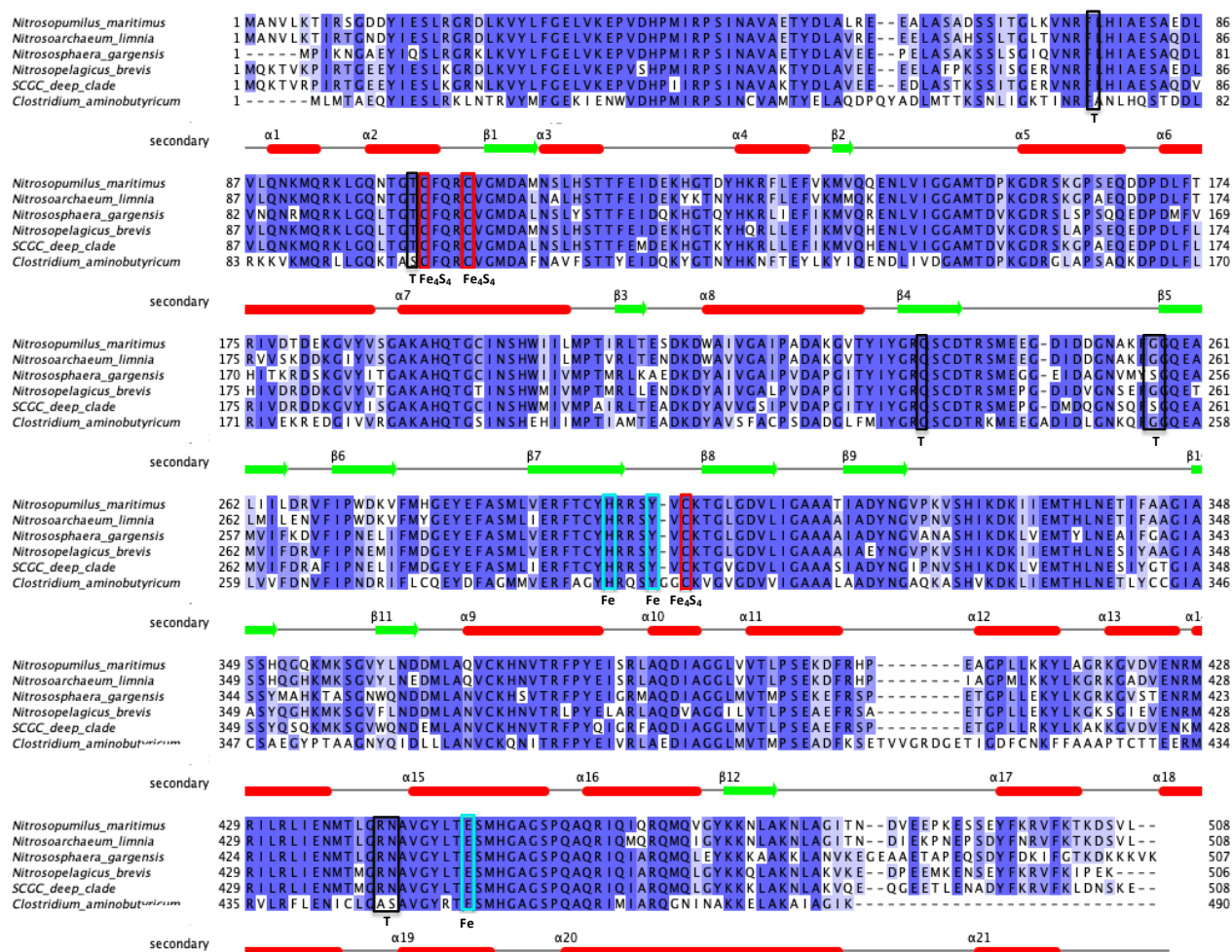
Figure 2. Alignment of 4-hydroxybutyryl-CoA dehydratase (4HBD) sequences from (anaerobic) *Clostridium aminobutyricum* **and five representative (aerobic) ammonia-oxidizing archaea.** These AOA sequences correspond to distinct ecotypes: *N. maritimus* SCM1 (marine), *Candidatus* Nitrosarchaeum limnium SFB1 (low-salinity), *Nitrososphaera gargensis* Ga9.2 (soil), *Ca.* Nitrosopelagicus brevis CN25 (oceanic water column group A, WCA), and a single-cell amplified genome 'SCGC_deep_clade' (oceanic water column group B, WCB). Secondary structure elements placed based on our *N. maritimus* (4HBD) structure. α-Helices are shown in red tubes and beta-strands in green arrows. Positions of important residues are indicated. The positions of catalytic cysteine residues that are involved in the [4Fe-4S] cluster coordination are enclosed by red rectangles. The positions of critical residues H195, Y299 and E449 that are involved in the catalytic Fe coordination enclosed by cyan rectangles. The positions of tunnel constriction residues T102, Q237, G257, G258, R441 and N442 on tunnel 1 and L77 on tunnel 2 are enclosed in black rectangles and indicated by letter "T" (see below and Figure 3).
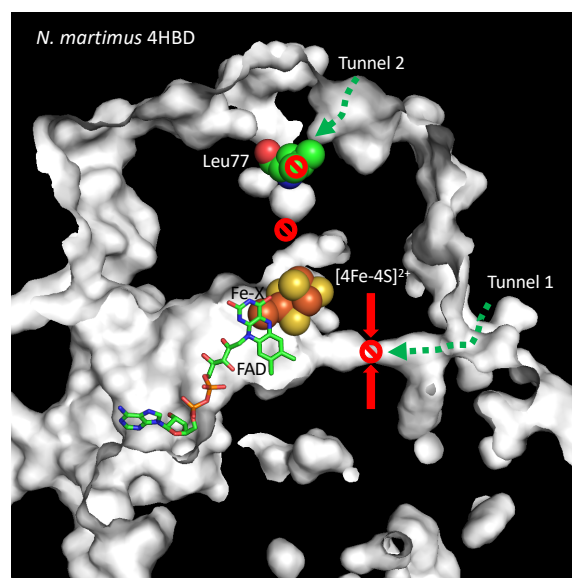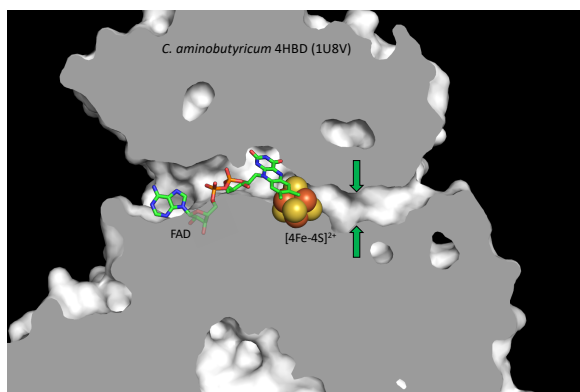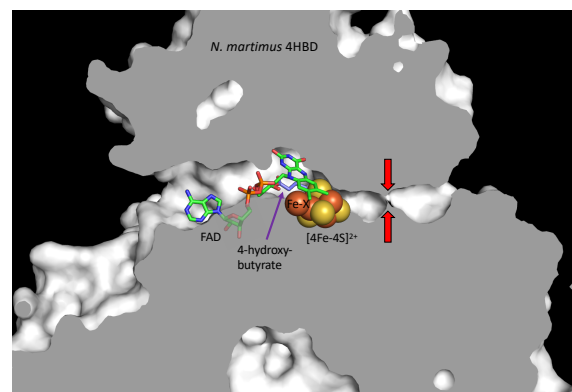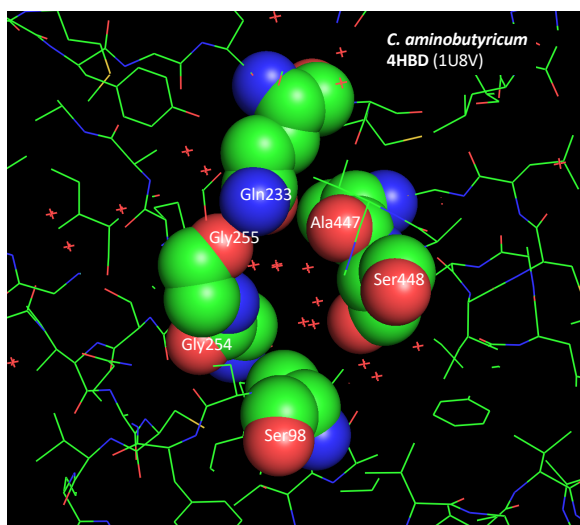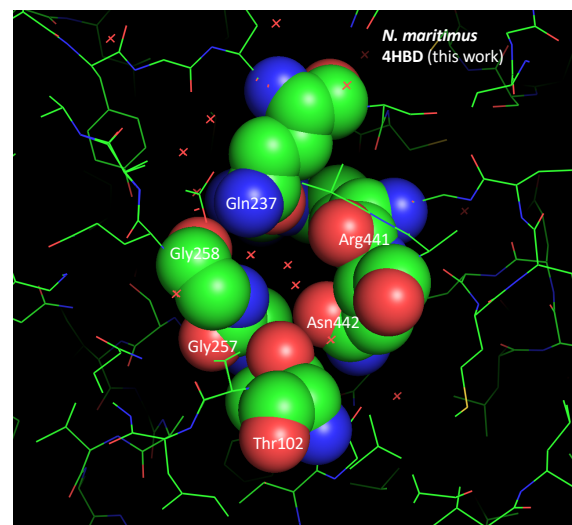
Figure 3. Active site tunnels reaching to the other side of the enzyme monomer likely controlling oxygen access A) Cross section of the tunnel in *C. aminobutyricum* going through the oxygen-sensitive 4HBD of active site connecting to the other side of the enzyme. The tunnel is open between the [4Fe-4S] cluster and the exit. B) Cross section of the tunnel of *N. maritimus* 4HBD including the enzyme's active site. Fe-X and [4Fe-4S] cluster are shown as spheres while FAD and the substrate analogue are depicted as stick models, the latter in purple. C) Cross section viewed after a 90 degree rotation around a horizontal axis in panel A. D) Cross section of *N. maritimus* 4HBD rotated by 90 degrees around the horizontal axis of panel B, showing the horizontal back channel closed in the middle. E) 6 residues forming the tunnel wall at the position, indicated by vertical green arrows in A, where the corresponding to the constriction in *N. maritimus* 4HBD. F) 6 residues constricting the back tunnel at one third of the way through the tunnel, as indicated by the red vertical arrows in B and D. In E and F, other protein amino acids are shown in wire models, and water molecules as red crosses. Panels A, C, and E are drawn using molecule D of *C. aminobutyricum* 4HBD (PDB 1u8v), and B, D, and F using molecule A of the *N. maritimus* 4HBD (this work).
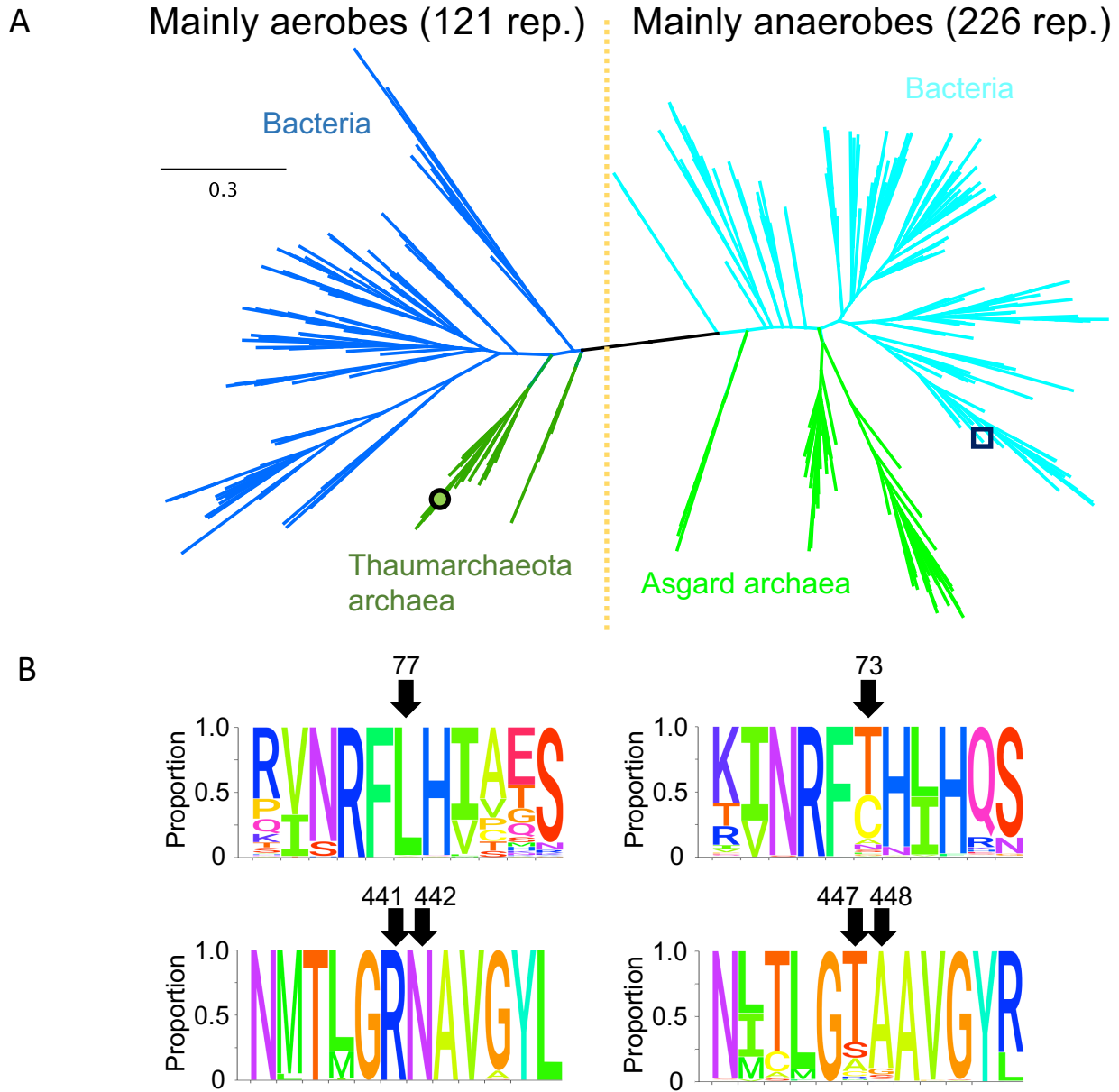
Figure 4. Phylogenetic analysis of the 4HBD sequences and residues constricting the back tunnels. A) Phylogenetic analysis of representative 347 4HBD homologues is shown. All sequences were first retrieved by BLASTP analysis using the Nmar 4HBD sequence as a query. We then eliminated the sequences that have length shorter than 80% of *N. maritimus* 4HBD and over 90% identity to any other sequences in the list. The 4HBD homologues derived from bacteria and archaea are shown in (dark and light) blue and (dark and light) green, respectively. The open circle and square indicate *N. maritimus* and *C. aminobutylicum* 4HB, respectively. B) The proportion of amino acid conservation for two constriction motifs corresponding to the back tunnels 1 and 2 are shown in the sequence logo at the bottom and top panels, respectively. The left panels correspond to these motifs from the clades primarily represented by aerobes. The numbers on the left panels denote the corresponding amino acid positions in the 4HBD of *N. maritimus*. The right panels correspond to these constriction motifs from the clades primarily represented by anaerobes, and the numbers denote the corresponding amino acid positions in the 4HBD of *C. aminobutyricum*.

22
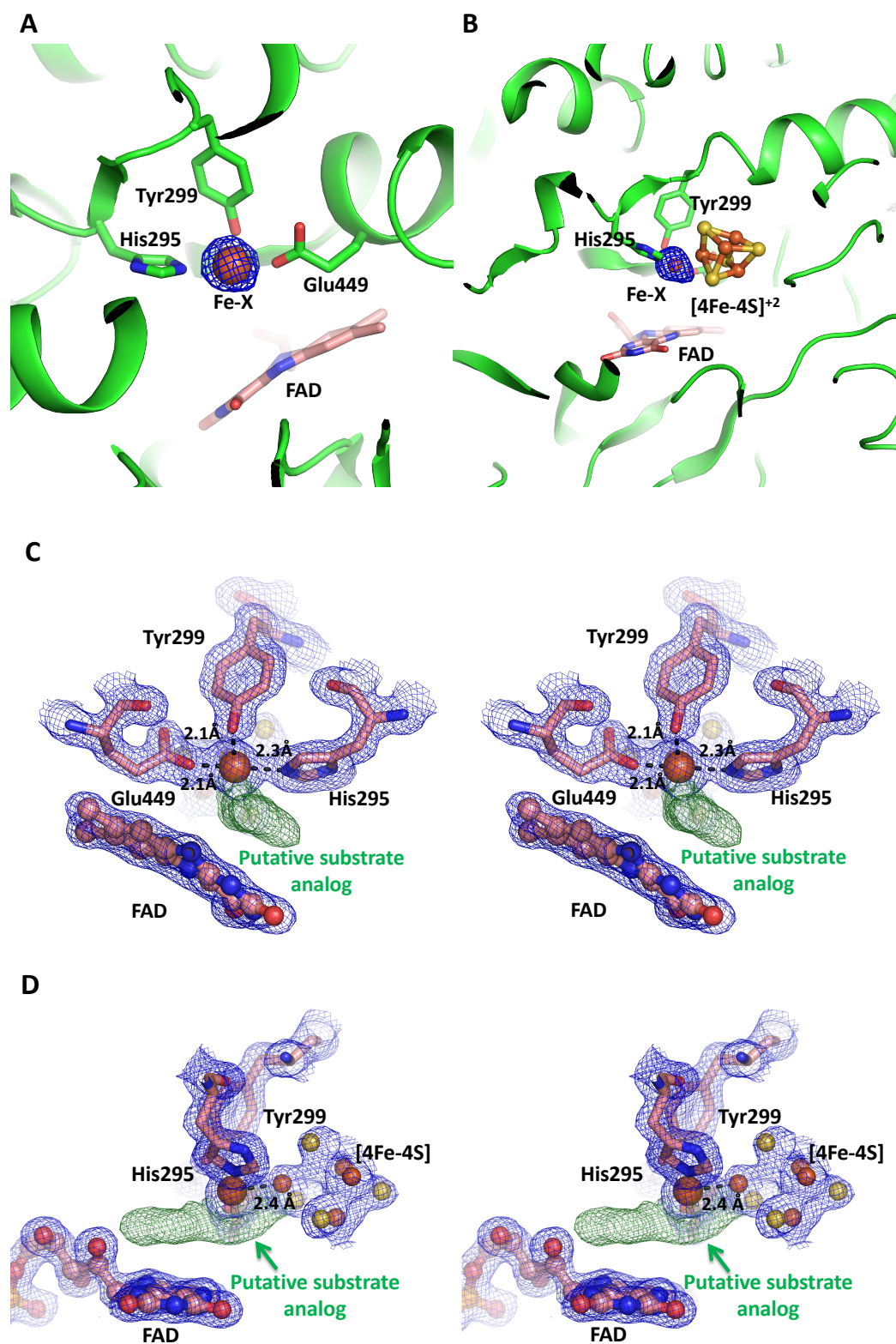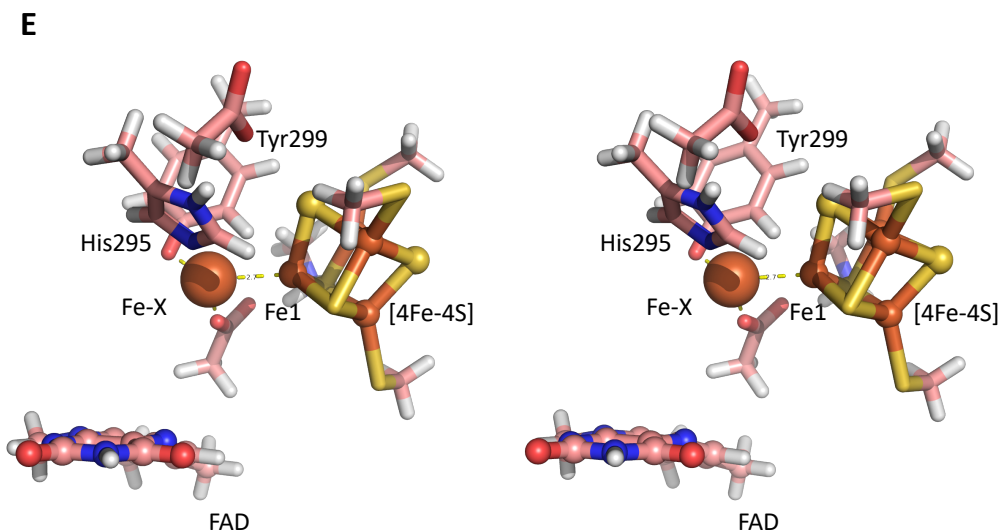
Figure 5. Active site of the *N. maritimus* 4-hydroxybutyryl-CoA dehydratase (4HBD). A) Anomalous electron density map of the active site Fe atom. Balls and sticks representation of the 4HBD chain A active site. The residues (H295, Y299, E449) and cofactor (FAD) are indicated with sticks. Experimental anomalous electron density map at the Fe K-edge is shown at 5 sigma level B) side view of panel A showing the [4Fe-4S] cluster and the anomalous electron density of the Fe-X. C) Active site structure and electron density map of the *N. maritimus* 4-hydroxybutyryl-CoA dehydratase (4HBD) shown in stereo diagrams. Balls and sticks representation of the 4HBD chain A active site. The positions of catalytic Fe residue is indicated by orange sphere. The residues (H295, Y299, E449), and cofactor (FAD) are indicated with sticks, and experimental 2Fo-Fc electron density maps are shown at 1.5 sigma level and carved at 3 Å from the non-hydrogen atoms and colored in blue. Experimental Fo-Fc difference electron density that is assumed to be putative substrate analog is shown at 3.0 sigma level and carved at 3 Å from non-hydrogen atoms and colored in green. D) Same as in panel C and rotated by about 90 degrees to give a better view of the [4Fe-4S] cluster, Fe-X and putative substrate analog (indicated by green arrow) with respect to the FAD isoalloxazine ring N5 nitrogen atom. E) Optimized geometry of the active site in stereo at the BP86/def2-svp level with the QM/MM methodology. Only the atoms treated in the quantum mechanical calculations including hydrogen atoms are shown, in a viewing angle similar to that of panels B and D.

24

SUPPLEMENTARY MATERIALS
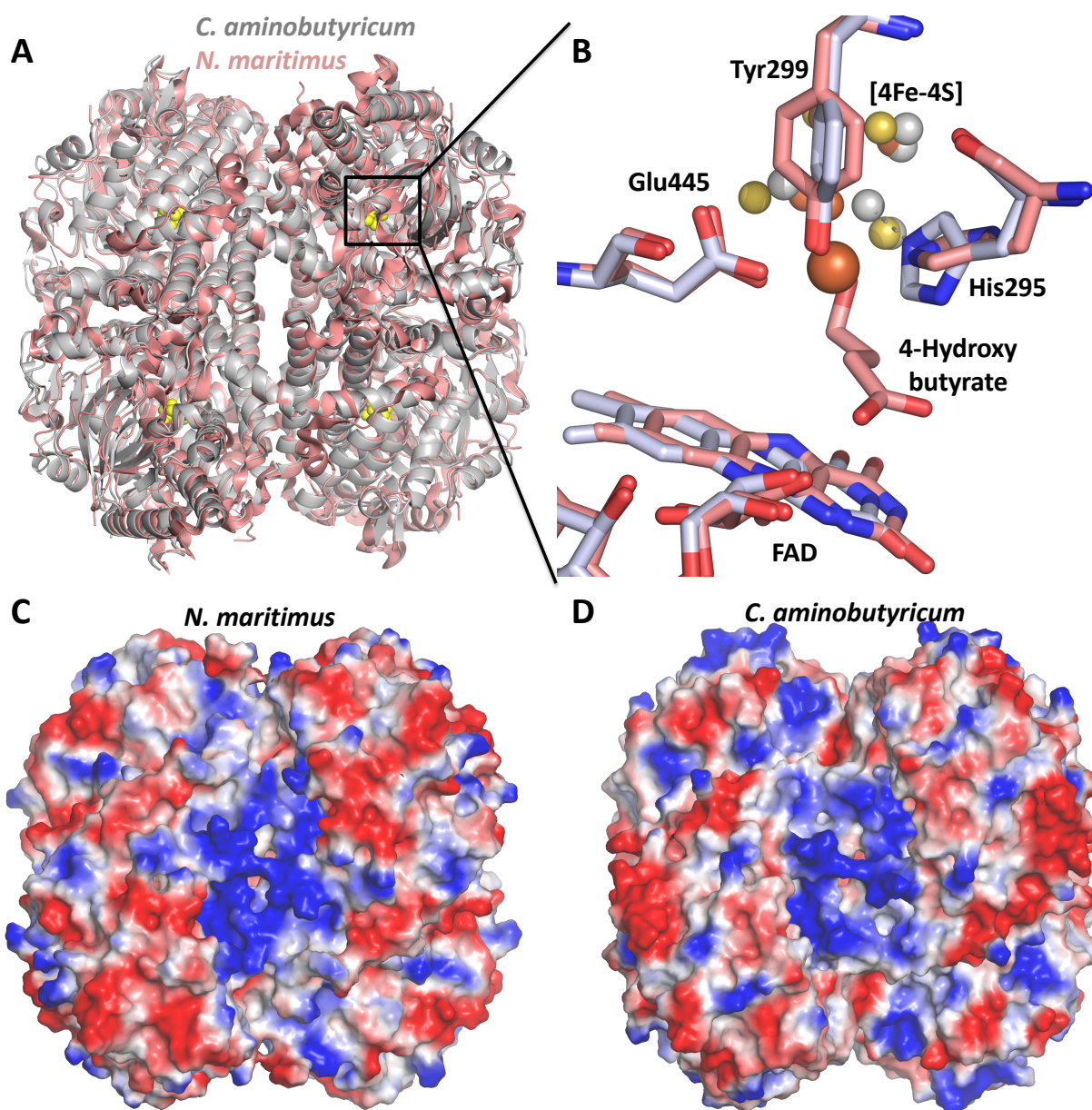
Supplementary Figure S1. Comparison of anaerobic bacterial vs aerobic archeal 4HBD structures. A) Cartoon representation of superimposed C. *aminobutyricum* and *N. maritimus* structures. The overall RMSD is 0.54 Å between all the Cα residues, which indicates a high similarity between the two structures. The only notable difference is the presence of a N- and C-terminal extensions in aerobic version. B) Shows the expanded version of the inset in panel A. Positions of active site residues E445, Y299, H295, FAD and [4Fe-4S] cluster are highly conserved. C) Surface charge distribution of the *N. maritimus* 4HBD. D) Surface charge distribution of *C. aminobutyricum* 4HBD
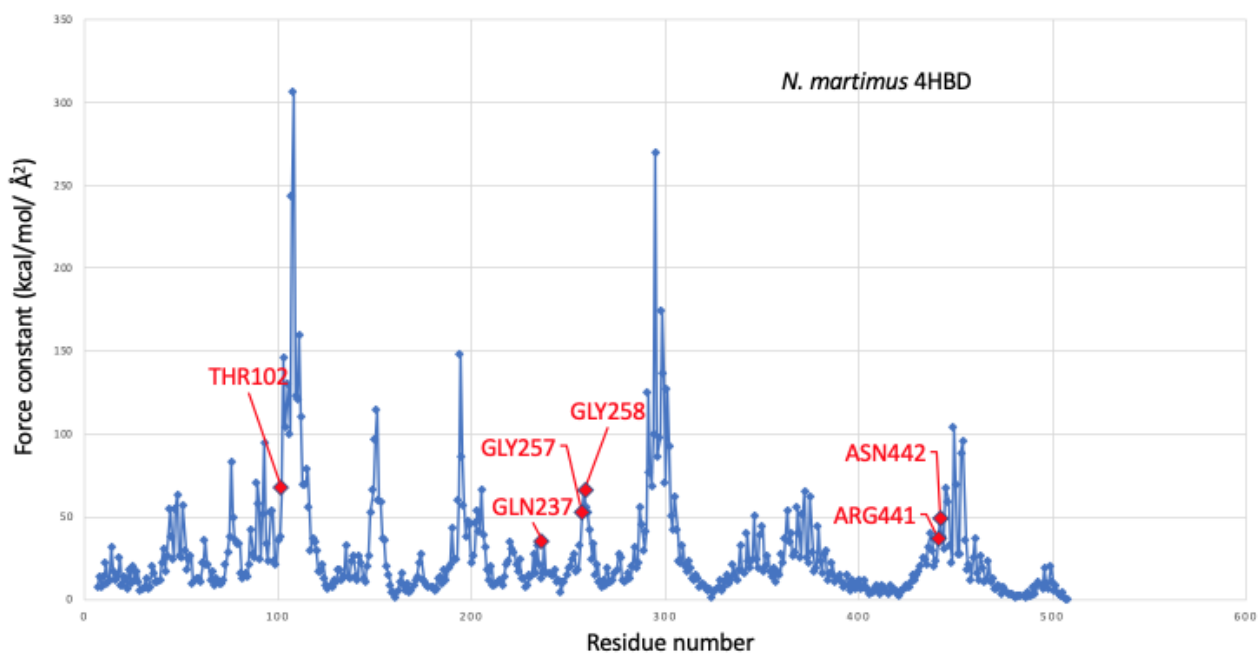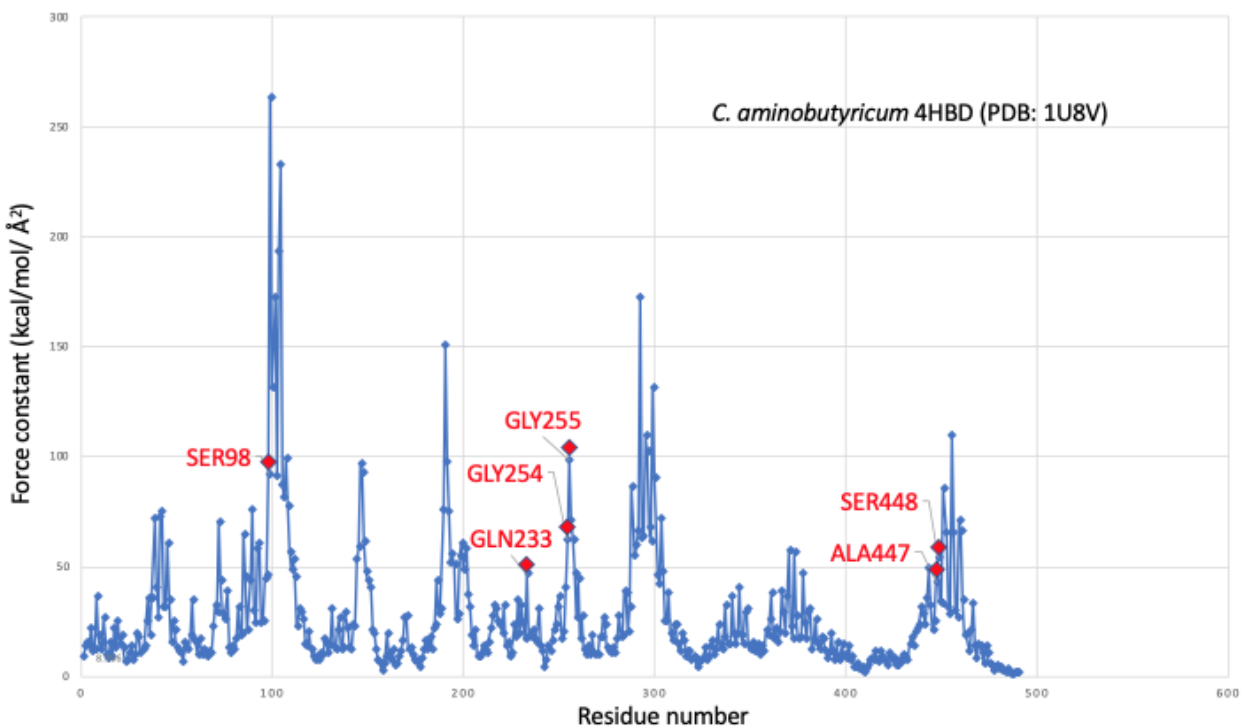
Supplementary Figure S2. Force constants of *C. aminobutyricum (upper panel)* and *N. maritimus* (lower panel) 4HBD calculated with ProPHet (http://bioserv.rpbs.univ-paris-diderot.fr/services/ProPHet/), showing the above average force constants for the residues forming the tunnel constriction.

Supplementary Table S1. Data collection and refinement statistics

	4HBD
Data collection	
Space group	$P2_1$
Cell dimensions	
a, b, c (Å)	87.5, 72.9, 180.6
α, β, γ (°)	90.0, 98.4, 90.0
Resolution (Å)	40.0 – 1.55
	(1.61 – 1.55)
R_{sym} or R_{merge}	0.16 (0.75)
$I / \sigma I$	13.5 (2.82)
Completeness (%)	97.8 (97.4)
Redundancy	6.6 (5.9)
Refinement	
Resolution (Å)	34.85 – 1.55
	(1.59 – 1.55)
No. reflections	318601 (22395)
R_{work} / R_{free}	0.16/0.17
No. atoms	
Protein	16148
Ligand/ion	272
Water	1734
B-factors	
Protein	21.37
Ligand/ion	39.44
Water	36.02
R.m.s. deviations	
Bond lengths (Å)	0.003
Bond angles (°)	0.63

*Single crystal used for 4HBD dataset.

**Values in parentheses are for highest-resolution shell.